Surface Science 624 (2014) 25–31

Contents lists available at ScienceDirect

Surface Science

journal homepage: www.elsevier.com/locate/susc

Ab initio and classical molecular dynamics simulations of N_2 desorption from TiN(001) surfaces

D.G. Sangiovanni [a,*], D. Edström [a], L. Hultman [a], I. Petrov [a,b], J.E. Greene [a,b], V. Chirita [a]

[a] Department of Physics, Chemistry and Biology (IFM), Linköping University, SE-58183 Linköping, Sweden
[b] Departments of Materials Science, Physics, and the Frederick Seitz Materials Research Laboratory, University of Illinois, Urbana, IL 61801, USA

ARTICLE INFO

Article history:
Received 5 December 2013
Accepted 17 January 2014
Available online 24 January 2014

Keywords:
N_2 desorption
Surface diffusion
Nitrides
Molecular dynamics simulations
Density functional theory
Vacancy formation

ABSTRACT

Ab initio molecular dynamics simulations based on density functional theory show that N adatoms are chemisorbed in threefold sites close to a N surface atom and between the two diagonally opposed neighboring Ti surface atoms on TiN(001). The most probable N adatom reaction pathway, even in the presence of nearby N adatoms, is for the N adatom and N surface atom pair to first undergo several exchange reactions and then desorb as a N_2 molecule, resulting in a surface anion vacancy, with an activation barrier E_{des} of 1.37 eV and an attempt frequency $A_{des} = 3.4 \times 10^{13}$ s^{-1}. E_{des} is essentially equal to the N adatom surface diffusion barrier, $E_s = 1.39$ eV, while A_s is only three to four times larger than A_{des}, indicating that isolated N adatoms migrate for only short distances prior to N_2 desorption. The probability of N_2 desorption via recombination of N adatoms on TiN(001) is much lower due to repulsive adatom/adatom interactions at separations less than ~3 Å which rapidly increase to ~2 eV at a separation of 1.5 Å. We obtain good qualitative and quantitative agreement with the above results using the modified embedded atom method potential to perform classical molecular dynamics simulations.

© 2014 Elsevier B.V. All rights reserved.

1. Introduction

Due to remarkable physical properties including high hardness and mechanical strength [1–3], chemical inertness [4–6], thermal stability [7], and electrical conductivity which varies from metallic to semiconducting [8–10], transition-metal (TM) nitride thin films are used in a wide range of applications: from wear-resistant protective coatings for cutting tools and engine components [11,12] to diffusion barriers in electronic devices [13]. The actual properties achieved by a given TM nitride film depend in large part on surface and microstructural evolution during reactive growth. That is, the properties depend on the reaction kinetics of nitrogen on the film surface during growth in excess N_2 partial pressure. Here, we use TiN as a model system and focus on nitrogen desorption pathways and kinetics on TiN(001).

Several *ab initio* studies [14–19], with only a few performed using *ab initio* molecular dynamics (AIMD) [20,21], have considered the interaction of TM nitride surfaces with environmental gases such as oxygen, nitrogen, hydrogen, and carbon dioxide. Density functional theory (DFT) is commonly used to calculate adsorbate potential-energy landscapes, minimum energy paths, and diffusion barriers on static surfaces. These calculations require knowledge of stable system configurations. Moreover, lattice vibrations at finite temperature will affect the magnitude of diffusion barriers. Molecular dynamics (MD) simulations, which model atomic motion and vibrations as a function of temperature, can reveal the existence of unexpected system configurations and reaction pathways. Highly computationally intensive MD based on DFT is the most accurate computational tool presently available for resolving the dynamics and kinetics of atomistic material processes.

DFT calculations, which provide a good compromise in terms of reliability vs. computational time, are widely applied in condensed matter physics. However, DFT has several limitations [22]. The approximations used in DFT for estimation of electron exchange and correlation energy are optimized to describe three-dimensional lattices. This means that the abrupt changes which occur in the electron density at surfaces can result in under- or over-estimation of surface/adsorbate bond strengths, and hence incorrect adsorption energies [23]. This, in turn, results in incorrect predictions for the relative stabilities of different adsorption sites [24] and, in DFT-based AIMD simulations of surface kinetics, in incorrect predictions of preferred adsorbate diffusion pathways and jump rates. However, if AIMD simulation results are consistent with those obtained from MD simulations based on empirical potentials, which do not consider electron–electron interactions, it is reasonable to assume that the agreement is not accidental, and that the theoretical predictions are reasonable representations of actual physical phenomena.

Several studies indicate that atoms adsorbed on a solid surface have a long-range oscillatory interaction, which, as function of decreasing separation changes from attractive to repulsive to attractive. This was first suggested by Grimley [25], who used *ab initio* calculations to probe the behavior of two hydrogen atoms chemisorbed on metallic surfaces. Einstein et al. [26], based upon a tight-binding analysis, showed that the oscillatory interaction between two adatoms adsorbed on a solid surface is a general phenomenon. Subsequent field-ion

* Corresponding author. Tel.: +46 13282478; fax: +46 13137568.
E-mail address: davsan@ifm.liu.se (D.G. Sangiovanni).

0039-6028/$ – see front matter © 2014 Elsevier B.V. All rights reserved.
http://dx.doi.org/10.1016/j.susc.2014.01.007

microscope experiments, carried out by Tsong [27] and by Watanabe and Ehrlich [28], verified the theoretical prediction for Re–Re, Re–Pd, W–Pd, and Ir–Ir metal-atom pairs adsorbed on W(110). Later, Lau and Kohn [29,30] reported that these interactions are repulsive or attractive depending on the nature of the adsorbate atoms and on the filling of surface electronic bands. Knowledge of the transition from, and absolute values of, repulsive to attractive lateral interactions between Sb adatom pairs on Si(001), based upon modulated-beam mass spectrometry and thermally stimulated desorption experiments, was found to be essential for understanding antimony dopant desorption kinetics during Si(001) molecular-beam epitaxy [31]. Repp et al. [32] demonstrated, using scanning tunneling microscopy to probe the dynamics of Cu adatoms on Cu(111) surfaces, that an accurate quantification of adatom/adatom interaction strength as a function of separation is necessary to understand the role of such effects on crystal growth.

It is generally assumed that N_2 loss during thin-film growth of TM nitrides such as TiN(001) occurs by adatom/adatom associative desorption [33–37]. However, N-adatom/N-adatom (N_{ad}/N_{ad}) pair-interactions on TiN(001) have not been rigorously assessed. Based upon DFT calculations, Graciani et al. [34] reported that N adatoms can recombine by overcoming a barrier of 0.11 eV. This value was determined by fixing the position of one N adatom atop a Ti terrace atom, while moving the other N adatom progressively closer by steps corresponding to second-neighbor distances (~3 Å). DFT calculation results by Gall et al. [33,38], however, showed that the minimum energy path for N diffusion on TiN(001) is along <110> via atop N-terrace positions, not crossing over Ti terrace atoms. This indicates that N adatom associative recombination is unlikely to occur following the pathway suggested by Graciani and coworkers.

Here, we determine stable adsorption sites, diffusion pathways, and migration rates of N adatoms, together with reaction pathways leading to the associative formation and desorption of N_2 molecules on TiN(001). We perform both *ab initio* and classical molecular dynamics (AIMD and CMD) simulations as a function of temperature T, in which interatomic forces are obtained from DFT and the modified embedded atom method (MEAM) potential optimized for TiN bulk and surface properties [39]. We find that the most stable sites for N adatoms on TiN(001) are threefold positions at the center of a triangle formed by a terrace N atom, with which the adatom forms a covalent bond, and the two neighboring Ti terrace atoms. Anchored to underlying N terrace atoms, N adatoms are significantly less mobile than Ti adatoms on TiN(001) [33,40], and migrate between threefold sites along <110> channels which requires breaking the bond with the initial N terrace atom and reforming it with the diagonally opposite terrace atom.

Strong N-adatom/N-surface-atom (N_{ad}/N_{surf}) bonding hinders N_{ad} surface diffusion, but favors N_{ad}/N_{surf} exchange. As observed in AIMD and CMD simulations, only three to four N_{ad} diffusion hops on TiN(001) are observed prior to N_{ad}/N_{surf} desorption as N_2 molecules with $E_{des} = 1.37$ eV, thus producing vacant anion sites in the TiN(001) surface. Moreover, we show that N_2 formation by N_{ad}/N_{ad} associative recombination is considerably less likely, with $E_{des} = 2$ eV. We obtain good qualitative and quantitative agreement between *ab initio* and classical predictions which allows us to determine the probabilities of N_{ad} diffusion, N_{ad}/N_{surf} exchange, and N_{ad}/N_{surf} molecular desorption, with corresponding activation energies and prefactors acquired from Arrhenius plots of the rate constant as a function of temperature for each event.

2. Computational details

MD simulations are performed within the microcanonical ensemble (NVE), while the substrate temperature is maintained constant via periodic rescaling of the atomic velocities, which mimics a canonical (NVT) sampling of configurational space [41]. Standard Verlet algorithms are used to integrate Newton's equations of motion at time intervals of 1 fs for both CMD and AIMD runs. CMD simulations are carried out by describing atomic interactions with the second-neighbor modified embedded atom method [42] potential as implemented in the large-scale atomic/molecular massively parallel simulator (LAMMPS) [43]. We use the TiN MEAM parameters from our previous publications [39,44,45], which were shown to yield adatom formation energies, diffusion barriers, and Ehrlich step-edge barriers that are consistent with experimental values [36,46,47]. AIMD simulations are accomplished with the VASP code [48], using the generalized gradient approximation (GGA) [49], and the projector augmented wave (PAW) [50] method. The Brillouin zone is sampled with $3 \times 3 \times 1$ k-point grids centered at the Γ point. At each time step, the total energy is evaluated to an accuracy of 10^{-5} eV/atom using a plane-wave energy cutoff of 400 eV.

N adatom dynamics on TiN(001) terraces are probed as a function of temperature on 3×3 TiN(001) surface unit cells. The substrate consists of three layers for a total of 108 atoms. The lateral size of the simulation cell is sufficient to avoid adatom self-interactions. During all MD runs, the bottom slab layer remains fixed. This does not affect the substrate temperature, which depends only on the atomic-motion translational degrees of freedom. AIMD simulation boxes contain six vacuum layers to prevent interaction between TiN(001) surface slab replicas along the [001] direction. At each temperature, the average Ti–N in-plane nearest-neighbor distance $<d_{NN//}>$ in the simulation slab is obtained accounting for the experimental TiN thermal expansion coefficient, 9.35×10^{-6} K^{-1} [7], by rescaling the 0 K $<d_{NN//}>$ value, 2.127 Å for DFT + GGA [51] and 2.121 Å for MEAM [39]. Rescaling of $<d_{NN//}>$ as a function of temperature is necessary to avoid spurious substrate strain effects on the adatom jump rate [52]. Prior to initiating each MD run, thermal oscillations in the adatom-free simulation slab are allowed to stabilize for five ps, a time interval sufficient to equilibrate the phonon modes in the system.

AIMD runs are performed at temperatures $T = 1200$, 1500, 1800, 2200, and 2500 K for a total simulation time of ~1 ns. With CMD, we perform ten runs each at $T = 1200$, 1500, 1800, 2000, 2300, and 2500 K. All results are stored in video files with a time resolution of 10 fs. Each CMD run is continued for the time required to observe N_2 desorption. From the combination of AIMD and CMD runs, we extract pathways, kinetic barriers, and attempt frequencies for N_{ad} diffusion among threefold surface sites, N_{ad}/N_{surf} exchange events, and N_{ad}/N_{surf} desorption.

We calculate average attempt frequencies $\overline{A}$ and activation energies $\overline{E}_a$ from linear interpolation of the logarithm of the rate coefficient $\overline{k}$ (average rate coefficients $\overline{k}$ are obtained from MD runs) as a function of the inverse temperature using the Arrhenius equation: $ln(\overline{k}(T)) = ln(\overline{A}) - \overline{E}_a/(k_B T)$. Data scatter κ, for which $\kappa = ln[k(T_i)]$, is characterized at each temperature T_i by a normalized Gaussian distribution function f, with maximum at $\overline{\kappa} = ln\left(\overline{k}\right)$, and width σ_κ (standard deviation): $f(\kappa, \overline{\kappa}, \sigma_\kappa) = \left[1/\left(\sigma_\kappa\sqrt{2\pi}\right)\right] exp\left\{-\left[(\kappa-\overline{\kappa})/\left(\sqrt{2}\sigma_\kappa\right)\right]^2\right\}$. The uncertainty σ_κ is estimated using the formula reported in reference [53]: $\sigma_\kappa = [ln(\overline{k}/k^{min}) + ln(k^{max}/\overline{k})]/2$, for which k_{min} and k_{max} are the extreme values for the rate coefficient k. Rate coefficients outside the range $[k^{min}, k^{max}]$ occur with negligible probability. The uncertainties σ_E and σ_A for calculated values of the average activation energy $\overline{E}_a$ and attempt frequency $\overline{A}$ correspond to the widths of the normal distributions $f(E_a, \overline{E}_a, \sigma_E)$ and $f\left(A, \overline{A}, \sigma_A\right)$. The latter are obtained from a linear interpolation of a large number of stochastically created $\{\kappa(T_i)\}$ data sets, $\{\kappa(T_i)\} = \{ln[k(T_1)], ln[k(T_2)], \ldots, ln[k(T_n)]\}$; at each temperature T_i, a $\kappa(T_i)$ value is selected with probability $f(\kappa, \overline{\kappa}, \sigma_\kappa)$. Accordingly, in the results and discussion section, predicted values of E_a and A are expressed as $\overline{E}_a \pm \sigma_E$, and $\overline{A} \pm \sigma_A$.

To assess the probability for N_2 molecule formation via associative adatom recombination, we carry out additional MD tests: ten 0.5-ns-runs with CMD, at each of the temperatures listed above, for a total

simulation time of ~20 ns, and eight AIMD runs at 2500 K for a total duration of ~50 ps. Using DFT and MEAM energy minimizations, we estimate the interaction energy between two N adatoms on TiN(001) as a function of their separation distance. DFT energy minimizations are calculated on $5 \times 5 \times 1$ k-point grids centered at the Γ point; the two adatoms are allowed to relax orthogonal to the surface, atoms in the two top slab layers are relaxed in all directions, and atoms in the bottom slab layer are maintained stationary. Hence, the N_{ad}/N_{ad} interaction energy E_{int} is obtained as:

$$E_{\mathrm{int}}(d=|\vec{r}_a-\vec{r}_b|) = E\left[\mathrm{TiN}(001)+\mathrm{N_{ad,a}}(\vec{r}_a)+\mathrm{N_{ad,b}}(\vec{r}_b)\right]+E[\mathrm{TiN}(001)]+ \\ -E\left[\mathrm{TiN}(001)+\mathrm{N_{ad,a}}(\vec{r}_a)\right]-E\left[\mathrm{TiN}(001)+\mathrm{N_{ad,b}}(\vec{r}_b)\right], \quad (1)$$

for which $\vec{r}_a$ and $\vec{r}_b$ are the in-plane surface positions of nitrogen adatoms $N_{ad,a}$ and $N_{ad,b}$ separated by distance d.

Charge transfer maps describing interactions between N adatom pairs are obtained from DFT calculations, in which the total charge transfer ρ_{tot} is a linear combination of four self-consistent electron densities ρ_i: $\rho_{tot} = \rho_1 + \rho_2 - \rho_3 - \rho_4$. ρ_1 is the charge density of the system (terrace + 2 adatoms), ρ_2 is the charge density of the terrace alone, and ρ_3 and ρ_4 are the charge densities of the (terrace + $N_{ad,a}$) and (terrace + $N_{ad,b}$) sub-systems. The atomic positions used in all charge density calculations are given by the spatial coordinates of the relaxed (terrace + 2 adatoms) system.

With CMD, we determine the effects of increasing the substrate slab thickness up to ten layers and the surface area up to 8×8 surface unit cells for a maximum size of 2560 atoms. We estimate that the increase in allowed phonon wavelengths associated with the larger substrate sizes results in activation energies and attempt frequencies decreasing by less than 10%. Similar variations are expected for AIMD. However, this would not change the relative occurrences of the adatom interaction, diffusion, and desorption events reported here, and hence does not affect our conclusions.

3. Results and discussion

3.1. Stable N adsorption site on TiN(001)

Based upon previous CMD simulations carried out at 1000 K [39], we reported that N adatoms on TiN(001) reside primarily in fourfold hollow sites (Fig. 1a). However, we show below that such sites are actually metastable.

DFT calculations performed by Gall and coworkers [33] indicate that the stable N adatom site on TiN(001) terraces at 0 K is a *threefold* position, at the center of a triangle formed by a N terrace atom and the two nearest Ti surface atoms, close to the N surface atom (Fig. 1b), while the fourfold hollow site position is metastable. To determine the stable N adatom position on TiN(001) at finite temperatures, we use AIMD simulation runs at $T = 1000$–2500 K in which the initial (x,y) coordinates of N adatoms are randomly chosen at a distance of ~2 Å above the surface. As predicted by DFT at 0 K, all N adatoms promptly move to a threefold site in which they bond to a N surface atom. Diffusion energy profiles obtained from DFT at 0 K, Fig. 9 in Reference [38], show that N adatom migration from a fourfold hollow to a threefold site has a barrier of only ~0.33 eV, while the reverse transition has a much higher barrier of 0.95 eV.

CMD simulations of TiN(001) thin film growth at 1200 K reveal that N atoms incident on the TiN(001) terrace bond to a terrace N atom [54], consistent with the above AIMD results. The energy stabilization gain for the N adatom in the threefold site vs. the fourfold hollow site, as estimated by MEAM energy minimizations, is 4.2 eV. While the numerical result is clearly too high, as discussed below, the trend is in agreement with DFT results at 0 K. MEAM calculations using the nudged elastic band (NEB) method [55,56] show that a N adatom placed in a

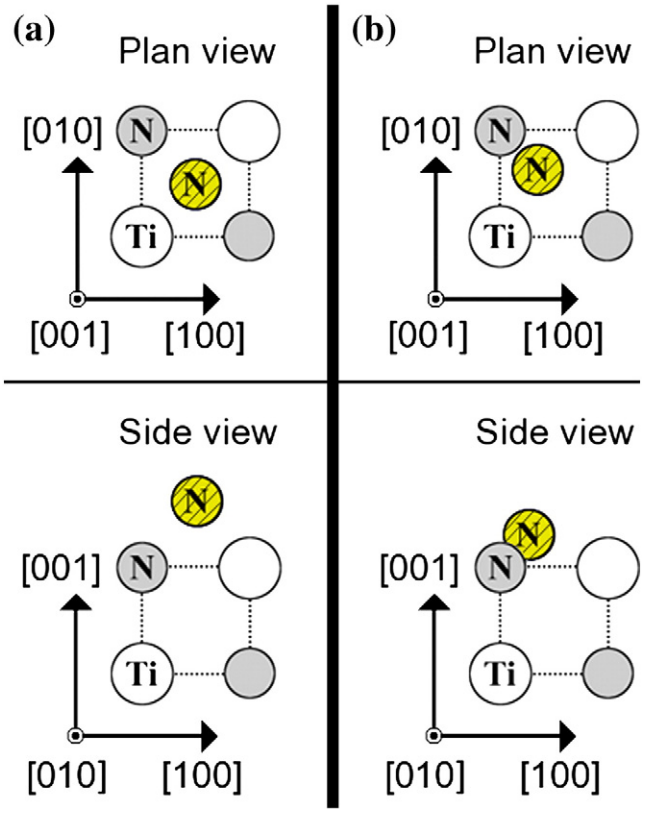

Fig. 1. N adatom (shown in yellow with cross-hatch) chemisorbed on TiN(001) in (a) a metastable fourfold hollow site and (b) a stable threefold site.

fourfold-hollow position at a distance of ~2 Å above the TiN(001) surface moves to the threefold position at a vertical distance of ~1 Å from the terrace with a barrier of 0.9 eV, while the reverse transition has an extremely high barrier of 5.1 eV (see Fig. 2a). However, the MEAM potential overestimates the N_{ad}/N_{surf} bond strength due to the limited amount of experimental information available for the N_2 gas reference system which is used to optimize N/N interactions within the MEAM formalism [57,58]

The N_{ad}/N_{surf} bond has a strong covalent character as shown by the marked electron accumulation shown in the DFT charge-transfer maps of Fig. 2b. During epitaxial TiN(001) growth by reactive magnetron sputter deposition [59], nitrogen precursors have average incident kinetic energies much higher than the barriers reported here for the N_{ad} transition from the fourfold hollow to the threefold site. Thus, the majority of N atoms, whether incident directly or provided by collisionally dissociated N_2 molecules, become trapped in threefold sites where they strongly bond to a N surface atom. Therefore, in the following CMD simulations, we focus on the dynamics of N atoms initially placed in threefold sites.

3.2. N adatom migration and desorption pathways on TiN(001)

In all AIMD and CMD runs, the N-adatom primarily moves from one threefold site to a neighboring threefold site via precession around a N surface atom through <100> channels (see Fig. 3a). Previous DFT calculations show that this surface diffusion pathway has a barrier of approximately 0.3 eV [33]. In our present AIMD simulations, we observe that the N adatom can also migrate to a diagonally adjacent threefold site by passing atop the N surface atom to which it is bonded. Neither pathway provides a significant contribution to intralayer mass transport, as the adatom remains proximate to the same N surface atom.

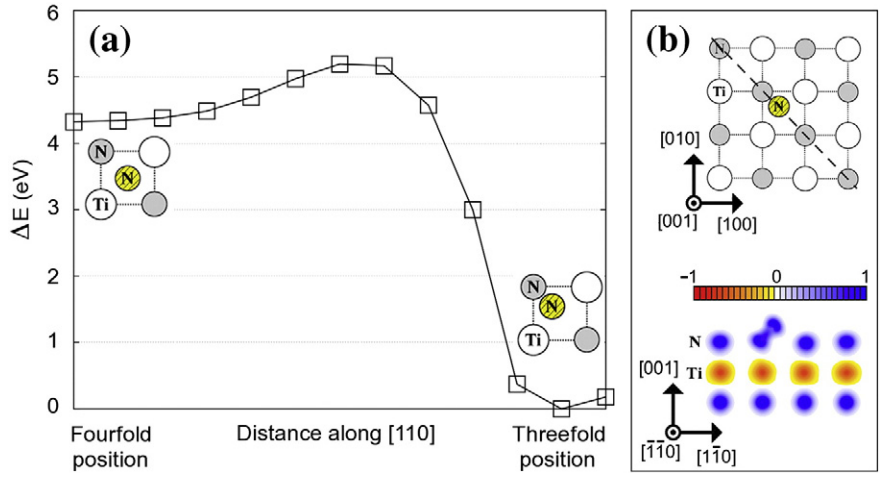

Fig. 2. N adatom diffusion on TiN(001). (a) Minimum energy ΔE path, calculated with MEAM + NEB, for N adatom migration from a metastable fourfold hollow site to a stable threefold site on TiN(001). ΔE is normalized to the energy of a N adatom in a threefold site. (b) A (110) charge-transfer map, oriented along the dashed line in the upper panel, showing covalent bonding between a N adatom in a threefold site and a N surface atom. The color scale is in electrons/Å^3 with blue indicating electron charge accumulation and red corresponding to charge depletion.

Our MD simulations show that N adatoms exchanging positions with N surface atoms (Fig. 3b) are highly likely events which are, however, not predictable by 0 K DFT calculations that only allow adatom surface migration [33]. In an exchange event, the N adatom moves downward and pushes the N surface atom into a stable threefold terrace site, maintaining the N_{ad}/N_{surf} bond. Exchange rates obtained from CMD simulations are plotted as a function of $1/T$ in Fig. 4a. The slope yields an exchange activation energy barrier $E_{ad/surf}$ of (0.54 ± 0.02) eV; an attempt

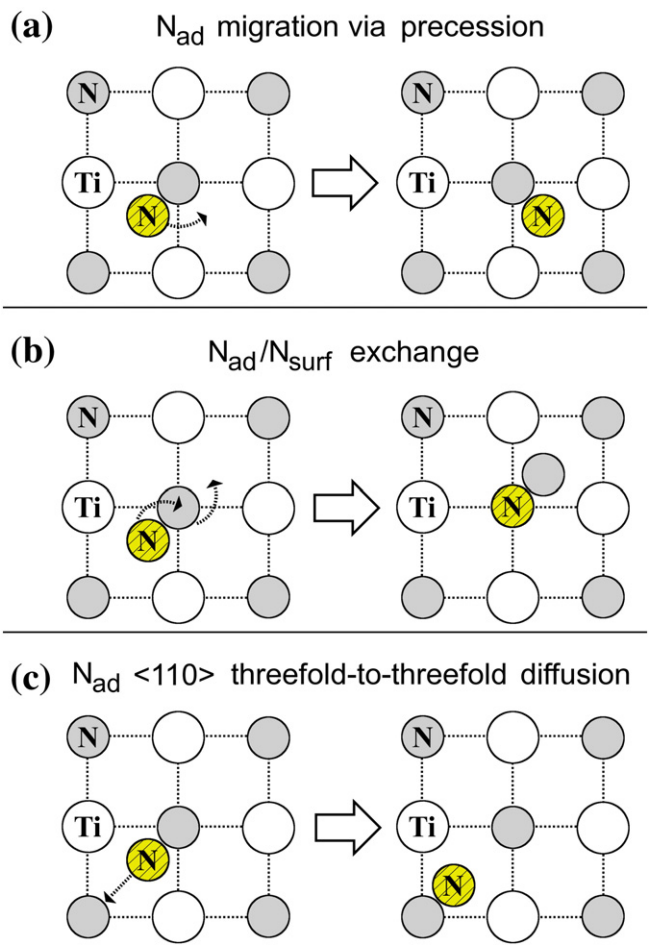

Fig. 3. N adatom (yellow with cross-hatch) migration on TiN(001). (a) N adatom precession between neighboring threefold sites located around a N surface atom. (b) A N-adatom/N-surface-atom (N_{ad}/N_{surf}) exchange event. (c) N adatom <110> diffusion through a fourfold hollow site to an adjacent threefold site.

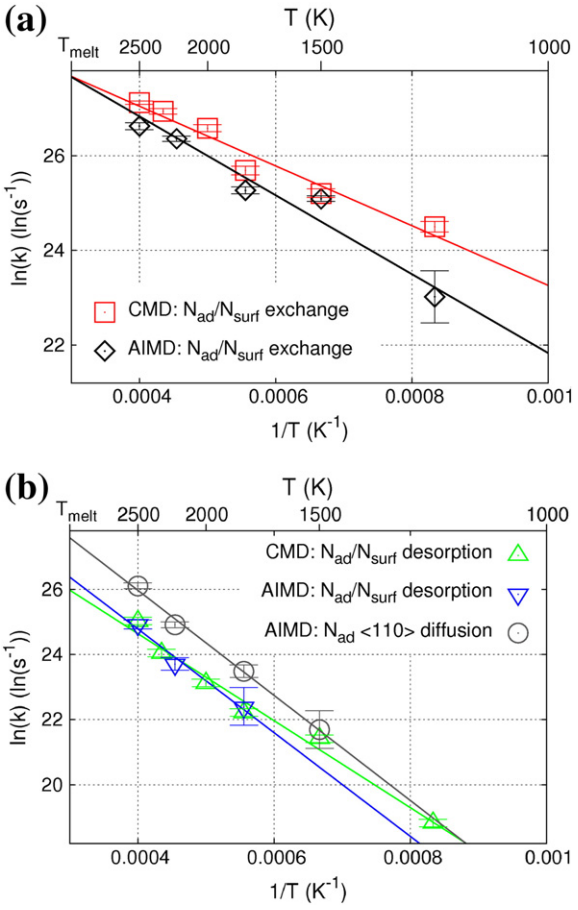

Fig. 4. Arrhenius plots for N adatom reactions on TiN(001) surfaces. (a) Rate constant k, calculated by AIMD and CMD, vs. $1/T$ for N-adatom/N-surface-atom (N_{ad}/N_{surf}) exchange. (b) N_{ad}/N_{surf} desorption rate constant k, calculated by AIMD and CMD, vs. $1/T$. The AIMD T-dependent N_{ad} <110> surface diffusion rate, from one threefold site to a diagonally adjacent threefold site (see Fig. 3c), is also shown. The error bars correspond to the uncertainty σ_{ln} (see text).

frequency $A_{ad/surf}$ of $(0.7 \pm 0.1) \times 10^{13}$ s^{-1} is obtained from the intercept of the curve with the vertical axis. AIMD results, also shown in Fig. 4a, yield $E_{ad/surf} = (0.69 \pm 0.09)$ eV and $A_{ad/surf} = (1.0 \pm 0.4) \times 10^{13}$ s^{-1}. NEB calculations for the N_{ad}/N_{surf} exchange mechanism provide activation energies of 0.42 eV (MEAM) and 0.60 eV (DFT). Previous *ab initio* 0 K calculations [34,37,60–62] have predicted strong bonding and adatom/surface exchange for chemisorbed oxygen and sulfur atoms on (001) TM nitride and carbide surfaces. This observation is supported by photoemission results for dissociatively chemisorbed O_2 and S_2 molecules on TiN, TiC, and ZrC (001) surfaces [34,60–63].

N adatoms can migrate from one threefold site to a neighboring threefold site by breaking and reforming N_{ad}/N_{surf} bonds (see Fig. 3c). In AIMD runs, each such event entails the N adatom moving first into the adjacent fourfold hollow site, then proceeding to the next threefold site, or returning to the original site. This pathway is never observed in our CMD runs, based upon the MEAM potential, due to the overestimated stability of N adatoms placed in threefold sites (see Section 3.1. and Fig. 2). From the AIMD Arrhenius plot shown in Fig. 4b, N_{ad} <110> threefold-to-threefold-site diffusion has an activation energy of (1.39 ± 0.15) eV with a prefactor of $(12.0 \pm 7.0) \times 10^{13}$ s^{-1}. We note that this barrier is nearly 50% larger than DFT predictions on static TiN(001) substrates of the same size [33], indicating that TiN(001) lattice vibrations significantly affect the energetics of N_{ad} migration. In our AIMD movies, we also observe that N adatoms located in metastable fourfold hollow sites can occasionally diffuse diagonally atop Ti terrace atoms to a neighboring fourfold hollow site. Such events occur in approximately 3% of the cases in which N adatoms occupy a fourfold hollow site at 2500 K. The low probability for this diffusion pathway can be explained based upon DFT adsorption energy landscape calculations. The fourfold-hollow to fourfold-hollow transition through an epitaxial site has an activation energy of ~0.6 eV, while the transition from a fourfold-hollow to a threefold site has a much lower barrier of only ~0.3 eV.

Our MD simulations reveal an unanticipated nitrogen desorption mechanism from TiN(001) surfaces: N_{ad}/N_{surf} molecular desorption (Fig. 5), which leaves a vacant anion site in the TiN(001) surface. Since in our CMD runs N adatoms retain unrealistically strong bonds with N terrace atoms, all CMD simulations end with N_{ad}/N_{surf} desorption and no N_{ad} surface migration. In AIMD runs, N adatoms typically perform three to four hops before N_{ad}/N_{surf} desorption is observed. In some cases, the desorption event appears to be activated by the N adatom migration itself, as the momentum transferred from a diffusing N_{ad} assists bond breakage between a N surface atom and neighboring Ti surface atoms. The N_{ad}/N_{surf} desorption rates estimated with AIMD/DFT and CMD/MEAM are in remarkable agreement (see Fig. 4b), demonstrating that our TiN MEAM potential [39] is reliable. Activation energies and attempt frequencies are $E_{des} = (1.37 \pm 0.30)$ eV and $A_{des} = (3.4 \pm 2.7) \times 10^{13}$ s^{-1} for AIMD and $E_{des} = (1.15 \pm 0.03)$ eV and $A_{des} = (1.1 \pm 0.3) \times 10^{13}$ s^{-1} for CMD. We note that the larger uncertainties for the AIMD values compared to the CMD values arise from the lower number of events recorded during AIMD runs.

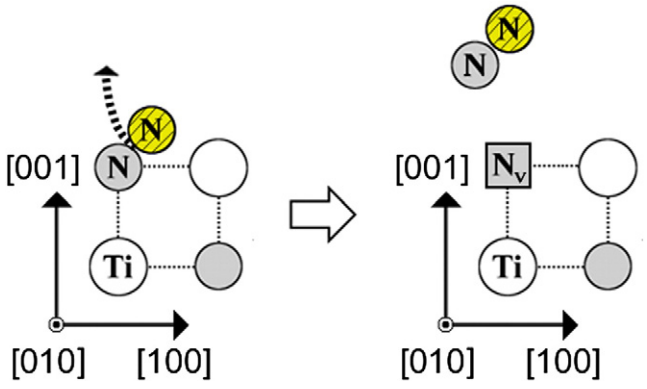

Fig. 5. Cross-sectional view illustrating N-adatom/N-surface-atom (N_{ad}/N_{surf}) molecular desorption. The N adatom is shown in yellow with cross-hatch. N_V is a surface anion vacancy site.

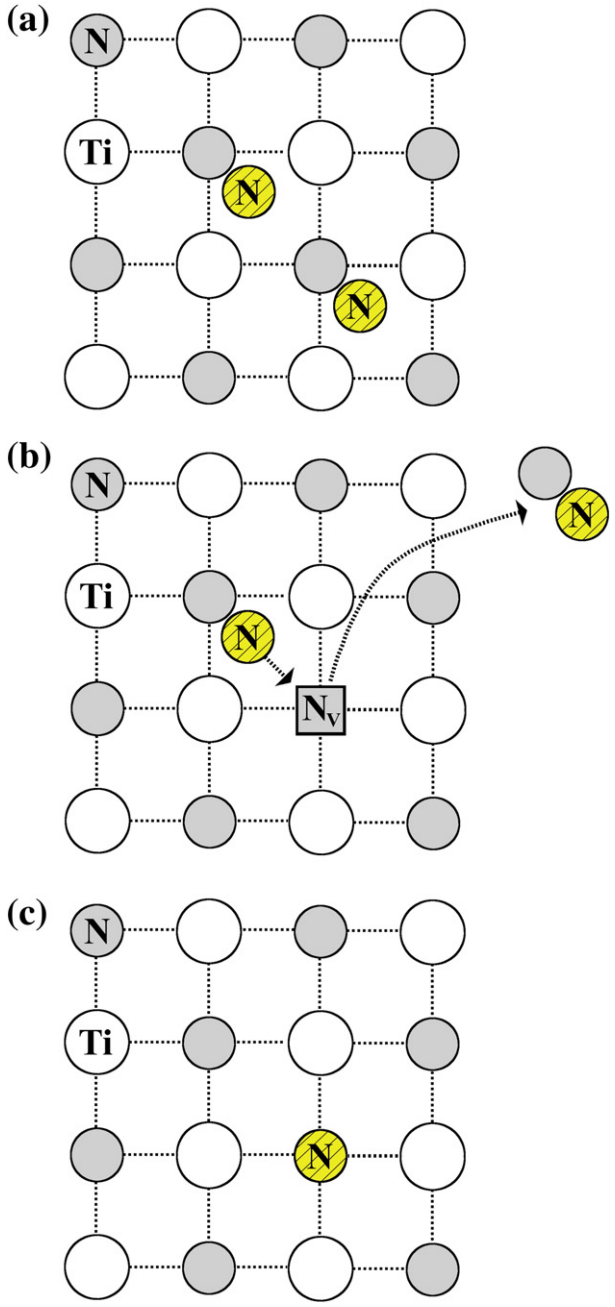

Fig. 6. N adatom behavior on TiN(001). (a) N adatoms (yellow with cross-hatch) occupying second-nearest-neighbor threefold sites on TiN(001). (b) Desorption of one of the N-adatom/N-surface-atom (N_{ad}/N_{surf}) pairs as a N_2 molecule leaving a surface anion vacancy N_V. (c) The remaining N_{ad} species diffuses along <110> to fill the surface vacancy.

Due to the use of periodic boundary conditions in our MD runs, desorbing N_2 dimers return to the TiN(001) substrate. In AIMD runs, dissociative chemisorption is never observed upon thermal N_2 gas collisions with a flat stoichiometric TiN(001) surface. On one occasion, however, a N_2 molecule stochastically collides with an anion vacancy site, giving rise to dissociation as one N atom occupies the anion vacancy and the other moves to an adjacent threefold site. This result suggests that anion vacancies can serve as catalysts for N_2 dissociative chemisorption. Vacancy-mediated dissociative chemisorption has been observed experimentally for H_2O and O_2 molecules on rutile-structure TiO_2(110) [64,65].

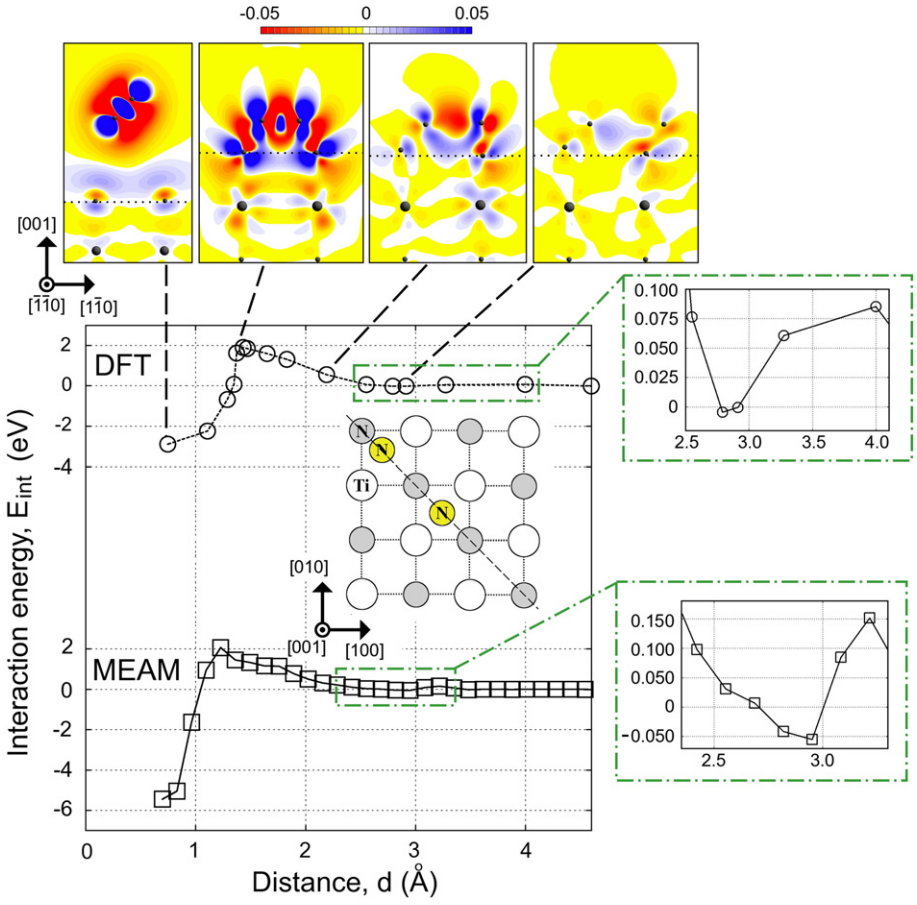

Fig. 7. Interaction energy E_{int}, calculated with both DFT and MEAM, as a function of the distance d between two N adatoms adsorbed on TiN(001). The exploded views in the rightmost panels reveal a small attractive interaction between N adatoms separated by distance $d \sim 3$ Å. The upper panels are (110) charge-transfer maps, oriented along the dashed line in the insert: small (large) filled black circles correspond to N (Ti) atoms, while the horizontal dotted line indicates the vertical position of the substrate surface layer. The color scale is in electrons/Å^3 with blue indicating electron charge accumulation and red corresponding to charge depletion.

A comparison between the AIMD rate constant vs. $1/T$ plots obtained for N_{ad} <110> threefold-to-threefold-site diffusion on TiN(001) and N_2 (N_{ad}/N_{surf}) desorption reveals that desorption occurs at approximately 1/3 the frequency of diffusion. Thus, isolated N adatoms migrate on TiN(001) for only very short distances (a few surface unit cells at most) before they form a N_{ad}/N_{surf} dimer and desorb. This observation reconciles the qualitative predictions of AIMD and CMD: AIMD results indicate that N adatoms have vanishingly small diffusivities on flat TiN(001) surfaces, while CMD simulations predict that isolated N_{ad} species chemisorbed in threefold terrace sites are immobile.

Even if two N adatoms are initially placed in parallel threefold sites in diagonally adjacent TiN(001) surface unit cells (see Fig. 6a), recombinatory N_{ad}/N_{ad} molecule formation leading to N_2 desorption is never observed in AIMD runs. In fact, AIMD movies show that N adatoms tend to diffuse away from each other by <110> migration, exchange positions with the N terrace atom to which they are bonded, or desorb as N_{ad}/N_{surf} dimers (see Fig. 6b). In the latter case, the remaining N adatom quickly diffuses into the vacated anion terrace site (Fig. 6c).

Since in CMD, N adatoms placed in threefold positions do not diffuse due to an overestimated N_{ad}/N_{surf} bond energy (see Fig. 2), CMD simulation tests are performed with the two N adatoms placed in neighboring metastable fourfold hollow sites. In all 60 tests (with a maximum duration of 0.5 ns each) carried out at $T = 1200$–2500 K, we never observe N adatom recombination; N adatoms diffuse away from each other along <110> channels crossing atop Ti terrace atoms as reported in Ref. [39]. All simulations performed at $T \geq 1800$ K ended with N_{ad}/N_{surf} pair formation and desorption.

Fig. 7 shows the interaction energies, calculated by both DFT and MEAM, between two N adatoms as a function of their interatomic distance on a TiN(001) surface. DFT energy minimizations are performed by fixing the in-plane position of one N adatom $N_{ad,a}$ at a stable threefold site $\vec{r}_a$, while varying the in-plane position $\vec{r}_b$ of the second adatom $N_{ad,b}$ along the diffusion pathway observed in AIMD movies, passing atop N terrace-atom positions. The same procedure is used in MEAM structural relaxations. However, in this case $N_{ad,a}$ is fixed in a metastable fourfold hollow site, while $N_{ad,b}$ samples sites along in-plane <110> directions passing atop Ti terrace atoms. DFT charge-transfer map calculations (as described in Section 2) are performed in order to observe changes in electron density distributions associated with N_{ad}/N_{ad} and N_{ad}/N_{surf} bonds as a function of $N_{ad,b}$ position (i.e., $N_{ad,a}$–$N_{ad,b}$ separation). In Fig. 7, the color code is defined such that blue and red represent electron density accumulation and depletion, respectively, corresponding to bond formation (blue) and destabilization (red).

Both DFT and MEAM calculations show that N adatoms placed on TiN(001) at distances larger than 4 Å exhibit negligible interaction (see Fig. 7). At separations of approximately 3 Å (which corresponds to the second-nearest-neighbor <110> distance on the TiN(001) surface), the two adatoms form a weak, long-range bond, as indicated by small interaction-energy minima, due to increased electron density between the N adatoms, in both DFT and MEAM results (see the exploded panels to the right in Fig. 7). At $N_{ad,a}$–$N_{ad,b}$ separations shorter than 3 Å, the interaction becomes repulsive, as both DFT and MEAM $E_{int}(d)$ curves move toward higher positive energies. In the charge-transfer map corresponding to d ~2 Å, there is a red electron depleted region (bond destabilization) between the N adatoms as well as between $N_{ad,b}$ and the adjacent terrace atoms. When the N adatoms are separated by $d = 1.5$ Å, the system reaches maximum $N_{ad,a}$–$N_{ad,b}$ repulsion,

with an interaction energy E_{int} ~2 eV, in both DFT and MEAM results. The E_{int} maximum stems primarily from strong destabilization of the chemical bonds formed between the adatoms and the N surface atoms. However, if the N adatoms have sufficient kinetic energy to overcome the repulsive force, a $N_{ad,a}/N_{ad,b}$ covalent bond starts to form at separations $d \lesssim 1.5$ Å, as indicated by the blue electron density accumulation region between the adatoms. This leads to N adatom recombination and desorption (see leftmost charge transfer map in Fig. 7). The rapidly decaying oscillatory trend in the DFT and MEAM N_{ad}–N_{ad} interaction energy on TiN(001) curves (Fig. 7) is consistent with those of previous theoretical and experimental studies for adatom pairs adsorbed on elemental metal surfaces [30,32,66].

The associative recombination of N adatoms on TiN(001) has a high activation energy of ~2 eV and hence a low probability of occurrence. Thus, in contrast to underlying assumptions of most experimental [35,36] and theoretical [33,34,37,67] investigations on reactive TiN(001) thin film growth, our results show that N_2 desorption from TiN(001), rather than being controlled by N_{ad}/N_{ad} recombination, is primarily due to N_{ad}/N_{surf} dimer formation and desorption which has a considerably lower activation barrier, ~1.4 eV. This observation, combined with our results for N_{ad} diffusion on TiN(001), demonstrating that N adatoms migrate only for very short distances on TiN(001) (a few unit cells at the most) before desorbing as N_{ad}/N_{surf} dimers, indicates that individual N adatoms provide a negligible contribution to intralayer mass transport on flat TiN(001) surfaces during reactive film growth. However, the resulting anion surface vacancies may have an effect on TiN nucleation and growth kinetics.

4. Conclusions

We use both AIMD, based on DFT, and CMD simulations to investigate the dynamics of chemisorbed N adatoms on TiN(001) at temperatures between 1200 and 2500 K. The stable adsorption site is the threefold position at the center of a triangle formed by a N terrace atom, with which N adatoms form a strong covalent bond, and the two neighboring Ti terrace atoms. Our results demonstrate that isolated N adatoms exhibit negligible diffusion on TiN(001), as they perform only three to four threefold-to-threefold surface migrations before desorbing as N_{ad}/N_{surf} molecules. The surface anion vacancy sites created in this process are traps for itinerant N adatoms and serve as catalysts for N_2 dissociative chemisorption. The associative recombination of N adatoms is considerably less likely than N_{ad}/N_{surf} molecular desorption on TiN(001). N adatom pairs exhibit in-plane oscillatory interactions along the lowest-energy diffusion pathway, which at separations of ~1.5 Å result in a strong repulsion energy of ~2 eV. Overall, temperature-dependent AIMD/DFT and CMD/MEAM simulation results are in good qualitative and quantitative agreement.

Acknowledgments

Calculations were performed using the resources provided by the Swedish National Infrastructure for Computing (SNIC), on the Triolith Cluster located at the National Supercomputer Centre (NSC) in Linköping and on the Akka and Abisko clusters located at the High Performance Computing Center North (HPC2N) in Umeå, Sweden. We gratefully acknowledge financial support from the Knut and Alice Wallenberg Foundation (isotope project), the Swedish Research Council (VR) Linköping Linnaeus Initiative LiLi-NFM (grant 2008-6572), and the Swedish Government Strategic Research Area Grant in Materials Science on Advanced Functional Materials.

References

[1] H. Holleck, J. Vac. Sci. Technol. 4 (1986) 2661.
[2] H. Ljungcrantz, M. Oden, L. Hultman, J.E. Greene, J.E. Sundgren, J. Appl. Phys. 80 (1996) 6725.
[3] J.E. Sundgren, H.T.G. Hentzell, J. Vac. Sci. Technol. 4 (1986) 2259.
[4] L.A. Donohue, I.J. Smith, W.D. Munz, I. Petrov, J.E. Greene, Surf. Coat. Technol. 94–5 (1997) 226.
[5] D. McIntyre, J.E. Greene, G. Hakansson, J.E. Sundgren, W.D. Munz, J. Appl. Phys. 67 (1990) 1542.
[6] P. Panjan, B. Navinsek, A. Cvelbar, A. Zalar, I. Milosev, Thin Solid Films 282 (1996) 298.
[7] L.E. Toth, Transition Metal Carbides and Nitrides, Academic Press, New York, 1971.
[8] H.S. Seo, T.Y. Lee, J.G. Wen, I. Petrov, J.E. Greene, D. Gall, J. Appl. Phys. 96 (2004) 878.
[9] C.S. Shin, S. Rudenja, D. Gall, N. Hellgren, T.Y. Lee, I. Petrov, J.E. Greene, J. Appl. Phys. 95 (2004) 356.
[10] D. Gall, I. Petrov, N. Hellgren, L. Hultman, J.E. Sundgren, J.E. Greene, J. Appl. Phys. 84 (1998) 6034.
[11] J.M. Molarius, A.S. Korhonen, E. Harju, R. Lappalainen, Surf. Coat. Technol. 33 (1987) 117.
[12] V.R. Parameswaran, J.P. Immarigeon, D. Nagy, Surf. Coat. Technol. 52 (1992) 251.
[13] M.A. Nicolet, Thin Solid Films 52 (1978) 415.
[14] S.V. Didziulis, K.D. Butcher, S.S. Perry, Inorg. Chem. 42 (2003) 7766.
[15] S.V. Didziulis, K.D. Butcher, Coord. Chem. Rev. 257 (2013) 93.
[16] L. Tsetseris, S. Logothetidis, S.T. Pantelides, Appl. Phys. Lett. 94 (2009) 3.
[17] M. Marlo, V. Milman, Phys. Rev. B 62 (2000) 2899.
[18] C. Ruberto, A. Vojvodic, B.I. Lundqvist, Solid State Commun. 141 (2007) 48.
[19] A. Vojvodic, C. Ruberto, B.I. Lundqvist, Surf. Sci. 600 (2006) 3619.
[20] D. Music, J.M. Schneider, New J. Phys. 15 (2013) 11.
[21] S. Piscanec, L.C. Ciacchi, E. Vesselli, G. Comelli, O. Sbaizero, S. Meriani, A. De Vita, Acta Mater. 52 (2004) 1237.
[22] A.V. Ruban, I.A. Abrikosov, Rep. Prog. Phys. 71 (2008) 046501.
[23] L. Schimka, J. Harl, A. Stroppa, A. Gruneis, M. Marsman, F. Mittendorfer, G. Kresse, Nat. Mater. 9 (2010) 741.
[24] P.J. Feibelman, B. Hammer, J.K. Norskov, F. Wagner, M. Scheffler, R. Stumpf, R. Watwe, J. Dumesic, J. Phys. Chem. B 105 (2001) 4018.
[25] T.B. Grimley, J. Am. Chem. Soc. 90 (1968) 3016.
[26] T.L. Einstein, J.R. Schrieffer, Phys. Rev. B 7 (1973) 3629.
[27] T.T. Tsong, Phys. Rev. Lett. 31 (1973) 1207.
[28] F. Watanabe, G. Ehrlich, Phys. Rev. Lett. 62 (1989) 1146.
[29] K.H. Lau, W. Kohn, Surf. Sci. 65 (1977) 607.
[30] K.H. Lau, W. Kohn, Surf. Sci. 75 (1978) 69.
[31] S.A. Barnett, H.F. Winters, J.E. Greene, Surf. Sci. 165 (1986) 303.
[32] J. Repp, F. Moresco, G. Meyer, K.H. Rieder, P. Hyldgaard, M. Persson, Phys. Rev. Lett. 85 (2000) 2981.
[33] D. Gall, S. Kodambaka, M.A. Wall, I. Petrov, J.E. Greene, J. Appl. Phys. 93 (2003) 9086.
[34] J. Graciani, J.F. Sanz, T. Asaki, K. Nakamura, J.A. Rodriguez, J. Chem. Phys. 126 (2007) 244713.
[35] N.C. Saha, H.G. Tompkins, J. Appl. Phys. 72 (1992) 3072.
[36] M.A. Wall, D.G. Cahill, I. Petrov, D. Gall, J.E. Greene, Surf. Sci. 581 (2005) L122.
[37] J. Graciani, J.F. Sanz, A.M. Marquez, J. Phys. Chem. C 113 (2009) 930.
[38] M.A. Wall, D.G. Cahill, I. Petrov, D. Gall, J.E. Greene, Phys. Rev. B 70 (2004) 035413.
[39] D.G. Sangiovanni, D. Edström, L. Hultman, V. Chirita, I. Petrov, J.E. Greene, Phys. Rev. B 86 (2012) 155443.
[40] D.G. Sangiovanni, D. Edström, L. Hultman, I. Petrov, J.E. Greene, V. Chirita, unpublished.
[41] M.P. Allen, D.J. Tildesley, Computer simulation of liquids, Oxford University Press, 1989.
[42] B.J. Lee, M.I. Baskes, Phys. Rev. B 62 (2000) 8564.
[43] S. Plimpton, J. Comput. Phys. 117 (1995) 1.
[44] In our CMD simulations, we use a LAMMPS ialloy parameter value = 0. In Ref. [57], ialloy = 2.
[45] D. Edström, D.G. Sangiovanni, L. Hultman, V. Chirita, I. Petrov, J.E. Greene, Ti and N adatom descent pathways to the terrace from atop two-dimensional TiN/TiN(001) islands(unpublished).
[46] S. Kodambaka, V. Petrova, A. Vailionis, P. Desjardins, D.G. Cahill, I. Petrov, J.E. Greene, Surf. Rev. Lett. 7 (2000) 589.
[47] S. Kodambaka, V. Petrova, A. Vailionis, I. Petrov, J.E. Greene, Surf. Sci. 526 (2003) 85.
[48] G. Kresse, J. Hafner, Phys. Rev. B 47 (1993) 558.
[49] J.P. Perdew, K. Burke, Y. Wang, Phys. Rev. B 54 (1996) 16533.
[50] P.E. Blöchl, Phys. Rev. B 50 (1994) 17953.
[51] D.G. Sangiovanni, V. Chirita, L. Hultman, Phys. Rev. B 81 (2010) 104107.
[52] H. Brune, K. Bromann, H. Roder, K. Kern, J. Jacobsen, P. Stoltze, K. Jacobsen, J. Norskov, Phys. Rev. B 52 (1995) 14380.
[53] T. Nagy, T. Turanyi, Int. J. Chem. Kinet. 43 (2011) 359.
[54] D. Edström, D.G. Sangiovanni, L. Hultman, I. Petrov, J.E. Greene, V. Chirita, unpublished.
[55] G. Henkelman, B.P. Uberuaga, H. Jonsson, J. Chem. Phys. 113 (2000) 9901.
[56] G. Henkelman, H. Jonsson, J. Chem. Phys. 113 (2000) 9978.
[57] Y.M. Kim, B.J. Lee, Acta Mater. 56 (2008) 3481.
[58] B.J. Lee, T.H. Lee, S.J. Kim, Acta Mater. 54 (2006) 4597.
[59] L. Hultman, S.A. Barnett, J.E. Sundgren, J.E. Greene, J. Cryst. Growth 92 (1988) 639.
[60] J.A. Rodriguez, P. Liu, J. Gomes, K. Nakamura, F. Vines, C. Sousa, F. Illas, Phys. Rev. B 72 (2005) 11.
[61] J.A. Rodriguez, P. Liu, J. Dvorak, T. Jirsak, J. Gomes, Y. Takahashi, K. Nakamura, J. Chem. Phys. 121 (2004) 465.
[62] J.A. Rodriguez, P. Liu, J. Dvorak, T. Jirsak, J. Gomes, Y. Takahashi, K. Nakamura, Phys. Rev. B 69 (2004) 10.
[63] R. Souda, T. Aizawa, S. Otani, Y. Ishizawa, C. Oshima, Surf. Sci. 256 (1991) 19.
[64] R. Schaub, P. Thostrup, N. Lopez, E. Laegsgaard, I. Stensgaard, J.K. Norskov, F. Besenbacher, Phys. Rev. Lett. 87 (2001) 4.
[65] P. Scheiber, A. Riss, M. Schmid, P. Varga, U. Diebold, Phys. Rev. Lett. 105 (2010) 4.
[66] P. Hyldgaard, M. Persson, J. Phys. Condens. Matter 12 (2000) L13.
[67] S. Mahieu, D. Depla, R. De Gryse, Modelling the Growth of Transition Metal Nitrides, Iop Publishing Ltd., Stockholm, SWEDEN, 2007.